

Impact of Atomistic Substitution on Thin-Film Structure and Charge Transport in a Germanyl-ethynyl Functionalized Pentacene

Jeni C. Sorli,[†] Qianxiang Ai,[‡] Devin B. Granger,[‡] Kaichen Gu,[†] Sean Parkin,[‡] Karol Jarolimek,[‡] Nicholas Telesz,[‡] John E. Anthony,[‡] Chad Risko,[‡] and Yueh-Lin Loo^{*,†,§}

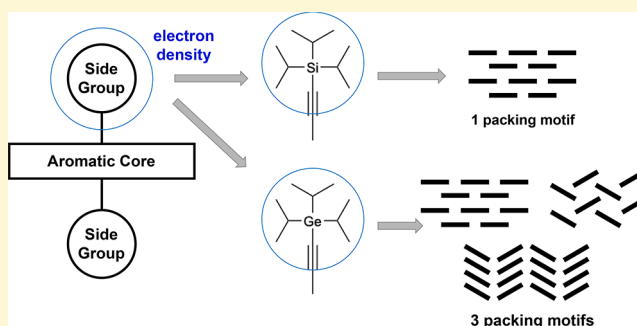
[†]Department of Chemical and Biological Engineering, Princeton University, Princeton, New Jersey 08544, United States

[‡]Department of Chemistry & Center for Applied Energy Research, University of Kentucky, Lexington, Kentucky 40506-0055, United States

[§]Andlinger Center for Energy and the Environment, Princeton University, Princeton, New Jersey 08544, United States

Supporting Information

ABSTRACT: Functionalization of organic semiconductors through the attachment of bulky side groups to the conjugated core has imparted solution processability to this class of otherwise insoluble materials. A consequence of this functionalization is that the bulky side groups impact the solid-state packing of these materials. To examine the importance of side-group electronic character on accessing the structural phase space of functionalized materials, germanium was substituted for silicon in triisopropylsilylethynylpentacene (TIPS-Pn) to produce triisopropylgermanylethynylpentacene (TIPGe-Pn), with the TIPGe side group comparable in size to TIPS, but higher in electron density. We find TIPGe-Pn single crystals exhibit slip-stack, herringbone, and brickwork packing motifs depending on growth conditions, a stark contrast to TIPS-Pn, which accesses only the brickwork packing motif in both single crystals and thin films. Polycrystalline thin films of TIPGe-Pn exhibit two new, unidentified polymorphs from spin-coating and postdeposition annealing. Our experiments suggest that access to the structural phase space is not guided solely by the size of the side group; the electronic character of the side group in functionalized compounds also plays a significant role. As such, simple atomistic substitutions can cause significant differences in the accessible solid structures.



INTRODUCTION

Charge transport in organic semiconductors requires, among many factors, sufficient electronic couplings among neighboring molecules; the solid-state molecular or their intermolecular packing can greatly impact electronic coupling and macroscopic electronic properties. It is therefore crucial to understand how organic semiconductors pack in the solid state and elucidate the processing–structure relationships that allow for controllable access to desired packing arrangements. The propensity for organic semiconductors to exhibit polymorphism, or access to distinct packing motifs, has necessarily complicated the compilation of such processing maps. Polymorphism is ubiquitous; nearly one-third of all organic substances display polymorphism under ambient conditions^{1,2} because the attractive intermolecular interactions, such as dispersion and electrostatic interactions, that hold these solids together are weak.³ Polymorphism has thus affected fields as wide ranging as pharmaceuticals and organic electronics, with strong influence over the stability or bioavailability of drugs and the charge transport properties of organic semiconductors, respectively.^{4–7} Specific to organic semiconductors, polymorphism of electrically active constituents has been shown

to critically impact the performance of transistors, ultimately varying field-effect mobilities by several orders of magnitude.^{8,9}

Because of the significant impact polymorphism has on the properties of organic semiconductors, methods of controlling molecular packing through processing have been developed. Structural control via conventional deposition methods, such as spin- or drop-casting, can be imparted in organic semiconductor thin films by tuning deposition conditions, such as solvent or spin speed.^{10,11} Introducing an external field, like blade-coating or dip-coating, can further result in preferentially aligned thin films.^{12–17} Additionally, postdeposition processing, such as solvent-vapor annealing or thermal annealing, has been shown to influence the final molecular packing. In some cases, postdeposition processing has provided access to different thin-film polymorphs.^{7,18–23} While the myriad deposition and postdeposition processing techniques have provided selectivity to the available packing motifs in thin

Special Issue: Jean-Luc Bredas Festschrift

Received: February 6, 2019

Revised: May 7, 2019

Published: May 8, 2019

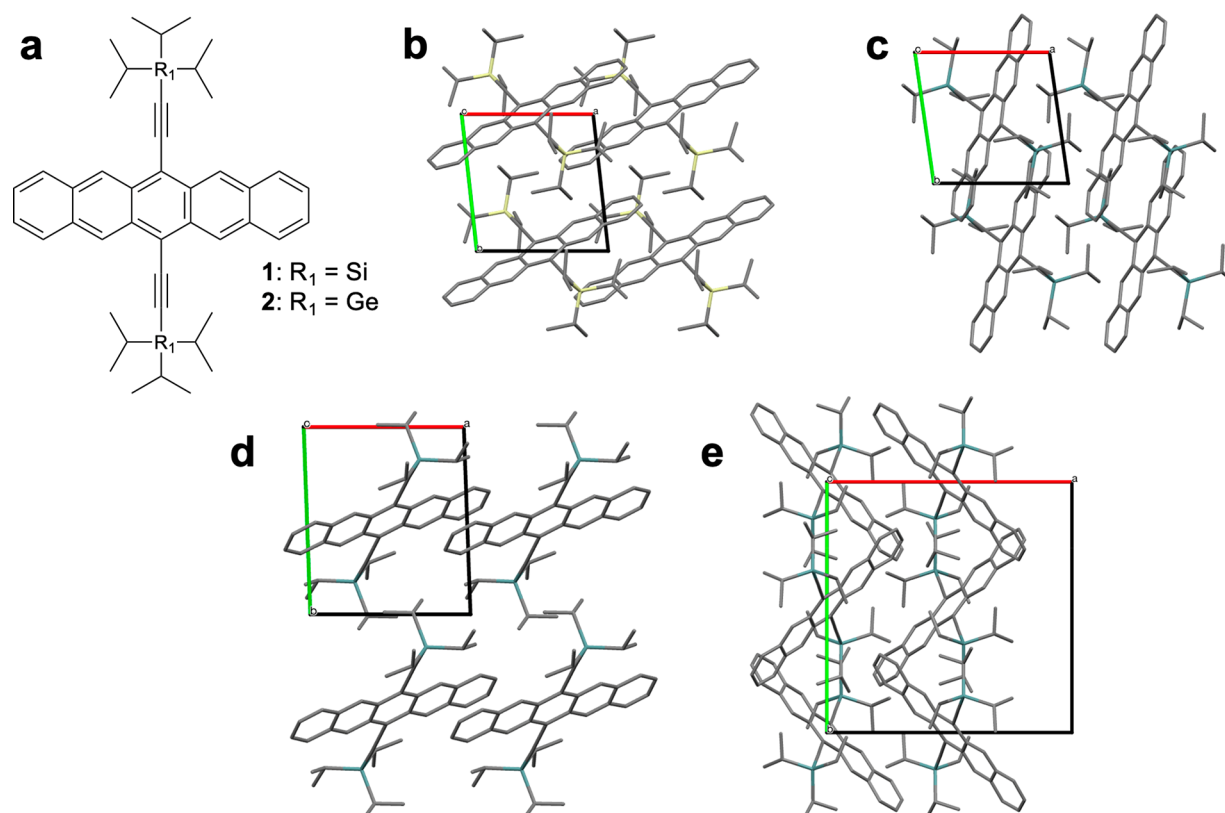


Figure 1. (a) Chemical structure of 6,13-bis(triisopropylsilylethynyl)pentacene, TIPS-Pn (1), and 6,13-bis(triisopropylgermanylethynyl)pentacene, TIPGe-Pn (2). Crystal structures revealing the (b) brickwork packing motif of TIPS-Pn (CCDC No. 172476²⁴) and the (c) brickwork, (d) slip-stack, and (e) herringbone packing motifs of TIPGe-Pn. All structures are viewed along their *c*-axes; hydrogen atoms are hidden for clarity.

films, the availability of packing motifs is ultimately dictated by the molecular structure of the compound studied. Understanding—and leveraging—molecular design to access desired structures and properties for organic semiconductor applications is therefore critical.

While there have been reports on tuning polymorphism with atomistic substitution directly of the conjugated core^{22,25} and with isomeric pairs,^{26,27} the influence that electrically inactive side groups and chains have on polymorphism is less explored. However, these substitutions are often incorporated to promote solubility and, accordingly, solution processability of the conjugated cores of organic semiconductors. Because these side groups and chains occupy space, their presence necessarily alters the packing motifs functionalized organic semiconductors adopt. Recently, the length of the side chain, size of the side groups,^{28–30} and atomistic substitutions^{31–33} have been shown to result in polymorphism in both molecular and polymeric semiconductors. In the specific case of functionalized acenes, pioneered by Anthony and co-workers, the bulky side groups have been shown to tune the solid-state packing motif, altering also intermolecular π -stacking and π -orbital overlap.²⁴ With 6,13-bis(triisopropylsilylethynyl)pentacene (TIPS-Pn), molecule 1 in Figure 1a, its TIPS substitution imposes a brickwork packing motif (Figure 1b), as opposed to the herringbone packing motif that is adopted by its unsubstituted pentacene counterpart.²⁴ Empirically, Anthony et al. proposed that brickwork packing motifs are accessed when the diameter of the alkyl substituent is approximately half that of the acene core length. Smaller substituents tend to result in compounds adopting a 1D slip-stack packing motif, as seen with 6,13-bis (triethylsilylethynyl)

pentacene (TES-Pn). Derivatives with substituent diameters significantly larger than half the size of the conjugated core exhibit hindered crystallization, the packing motif of which then becomes challenging to predict a priori. While these general principles have been widely leveraged to tune the intermolecular packing of conjugated acenes,³⁴ notable exceptions exist. Recent density functional theory (DFT) calculations by Thorley et al., for example, showed that the effective radii, the average distance between silicon and the outermost hydrogens of the side group, of TES- and TIPS-Pn are very similar, 3.88 and 3.89 Å, respectively, suggesting that the size of the side group cannot solely control the selectivity of packing motif.³⁵ The authors additionally suggested that the electron density of the side groups, found to be 28% higher for TIPS than TES, may also influence intermolecular interaction energies and determine the packing motif of these molecules.³⁵ To directly probe this hypothesis, we synthesized and characterized 6,13-bis(triisopropylgermanylethynyl)pentacene (TIPGe-Pn) to test the impact of side-group electron density on packing motif in functionalized pentacenes. While bulk crystals of TIPGe-Pn grown from solution typically show an edge-to-face (herringbone) motif (Figure 1e) with insignificant intermolecular π - π contacts suggesting poor charge-transport properties, recent results using this material in electronic radiation detectors suggest that the thin-film form must be substantially different from the bulk.³⁶

In this work, we probed how atomistic substitution of the alkyl substituent impacts the polymorphic landscape in thin films of TIPGe-Pn, in which the silicon atoms of the TIPS side group in TIPS-Pn are replaced with germanium. The substitution of germanium in TIPGe-Pn results in only a

Table 1. Packing Parameters and Cohesive Energies of TIPS-Pn and TIPGe-Pn Crystal Structures

molecule	packing	long axis slip (Å)	short axis slip (Å)	vertical slip (Å)	cohesive energy (eV/molecule)
TIPS-Pn	brickwork	9.51	1.88	3.22	2.453
		6.69	1.11	3.35	
TIPGe-Pn	brickwork	9.43	1.83	3.26	2.447
		6.89	1.24	3.36	
	slip-stack	7.54	2.20	3.44	2.642
	herringbone	N/A	N/A	N/A	2.656

0.07 Å, or 2%, increase in side-group radius relative to the triisopropylsilyl group of TIPS-Pn, but this substitution increases the electron density of the side group by 21%. Were the packing motif of these molecules determined solely by size exclusion, we would expect TIPGe-Pn to adopt a brickwork packing motif similar to that of TIPS-Pn.

We instead find this simple chemical substitution to result in a substantially wider phase space that is accessed in both bulk crystal and thin-film formats with TIPGe-Pn compared to TIPS-Pn. TIPS-Pn always accesses a brickwork packing motif in both bulk crystals and thin films, regardless of deposition and/or postdeposition processing conditions. We find that TIPGe-Pn accesses three distinct structures in bulk crystals: two polymorphs in spun-cast films that are yet different from those accessed in the bulk and a polymorph in aligned drop-cast films that is similar to the brickwork packing motif accessed in the bulk. The presence of several packing motifs in TIPGe-Pn relative to the single packing motif accessed in TIPS-Pn definitively implicates the role of electron density of the bulky side group in controlling solid-state structuring, and by implication, its electrical properties. We find thin-film transistors comprising spun-cast TIPGe-Pn active layers to exhibit poor charge transport, with mobilities on the order of $10^{-5} \text{ cm}^2 \text{ V}^{-1} \text{ s}^{-1}$ in the best case, regardless of the polymorph accessed. Thin-film transistors with active layers that access the brickwork packing motif exhibit mobilities of $0.72 \pm 0.21 \text{ cm}^2 \text{ V}^{-1} \text{ s}^{-1}$, comparable to those exhibited by aligned thin-film transistors of TIPS-Pn. Our findings highlight the importance of side-group electron density in addition to size in impacting the diversity of packing motifs accessed in functionalized organic semiconductors.

RESULTS AND DISCUSSION

The synthesis of TIPGe-Pn, molecule **2** in Figure 1a, was carried out following previously reported synthetic procedures for functionalized pentacenes via the Grignard reaction.^{34,37–40} The substitution of germanium for silicon in the alkyl substituent increases its effective radius by only 0.07 Å (from 3.86 Å for the triisopropylsilyl group to 3.93 Å for the triisopropylgermyl group), as determined by DFT calculations (see the Supporting Information).³⁵ This atomistic substitution in the alkyl substituent results in a trivial change in the van der Waals (VDW) volume of the sphere that it occupies, from 179.2 Å³ to 181.7 Å³ for the triisopropylsilyl and triisopropylgermyl groups, respectively. If size exclusion were the dominant driving force dictating solid-state packing motif, TIPGe-Pn should access a brickwork packing motif similar to that accessed by TIPS-Pn. Differentiating TIPGe-Pn and TIPS-Pn, however, is their electron densities, with germanium substitution increasing the electron density of the substituent by 21%. As dispersion forces are related to the electron density, a comparison of the packing motifs accessed by this pair of

organic semiconductors should shed light on the importance of substituent electron density on solid-state structuring.

We find that TIPGe-Pn exhibits a substantially richer phase space than TIPS-Pn; bulk crystals of TIPGe-Pn exhibit three distinct packing motifs. The crystal structures of TIPGe-Pn with brickwork, slip-stack, and herringbone packing motifs are shown in panels c, d, and e of Figure 1, respectively. The unit-cell parameters and CCDC numbers for these structures are included in Table S1, and details for crystal growth can be found in the Supporting Information. The packing parameters of these crystal structures, as well as those of the crystal structure of TIPS-Pn, are described in Table 1. We include the long, short, and vertical axis slips of each structure, which are all described relative to the pentacene backbone, with slip quantifying the translational displacement along these different axes between adjacent molecules. The slips along the long, short, and vertical axes of TIPS-Pn and TIPGe-Pn are similar, when they both adopt the brickwork packing motif. When TIPGe-Pn adopts the slip-stack packing motif, the crystal structure of which is shown in Figure 1d, the layered structure is more compressed and the side groups are interdigitated, leading to a decreased slip along the short axis (Table 1). Because of the face-to-edge orientation of the neighboring pentacene backbone in its herringbone packing motif (Figure 1e), slip axes cannot be defined for this motif. To further explore the intermolecular interactions in these packing motifs, the cohesive energy of each structure was calculated via DFT; these are also included in Table 1. Our calculations indicate the herringbone packing motif to be the most stable for TIPGe-Pn, with a cohesive energy of 2.656 eV/mol. This observation is consistent with us natively accessing the herringbone packing motif in bulk crystals of TIPGe-Pn when grown in solution. The cohesive energy of the slip-stack packing motif of TIPGe-Pn is slightly lower than that of the herringbone, at 2.642 eV/mol. At 2.447 eV/mol, the cohesive energy of the brickwork packing motif of TIPGe-Pn is approximately 200 meV smaller than both that of the slip-stack and herringbone motifs of TIPGe-Pn, suggesting the brickwork packing motif to be the least stable of the packing arrangements accessed. Interestingly, the cohesive energy of the brickwork packing motif of TIPGe-Pn is comparable to that of TIPS-Pn, at 2.453 eV/mol. Differential scanning calorimetry (DSC) thermograms for the brickwork and herringbone bulk crystals are included in Figure S1. Both crystals undergo a first-order phase transition upon initial heating, with peak enthalpies at 137 and 140 °C for the brickwork and herringbone packing motifs, respectively. While the difference in transition temperature is small, this difference suggests that TIPGe-Pn, in its herringbone packing motif, is more stable than TIPGe-Pn in its brickwork packing motif, an observation that corroborates the cohesive energy calculations above. The stability of the herringbone motif likely derives from the face-to-edge orientation of the pentacene backbone,

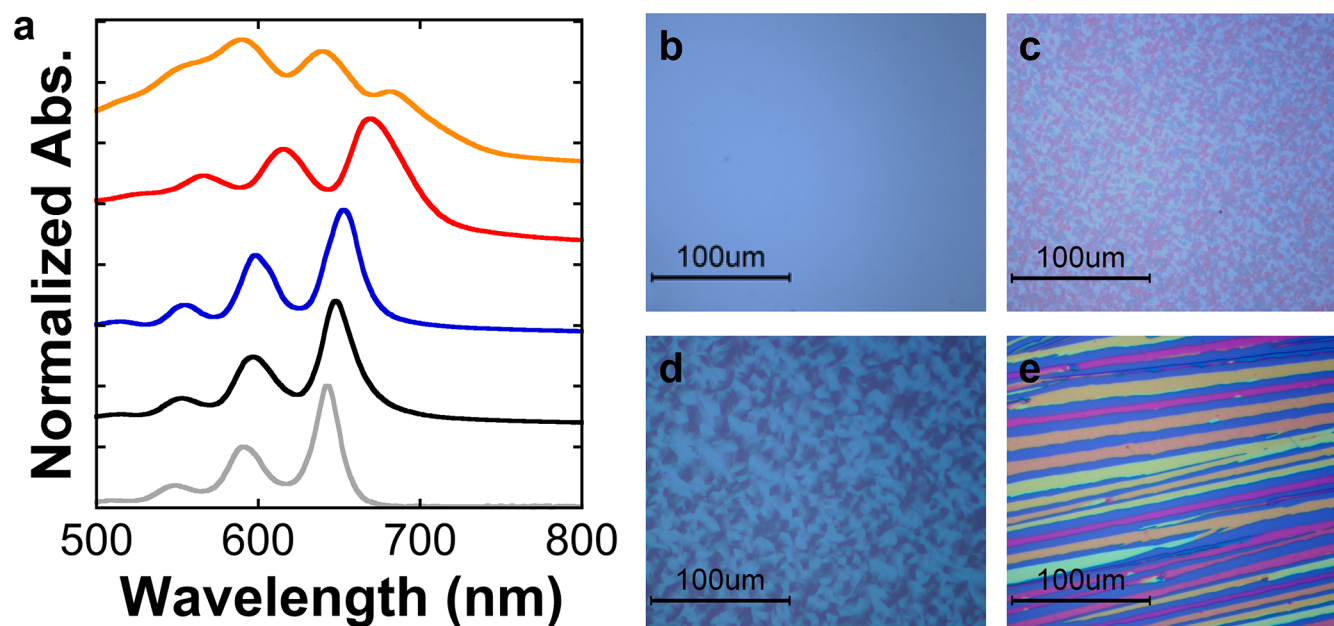


Figure 2. (a) UV–vis absorption spectra of TIPGe-Pn solution (gray trace); spun-cast thin films of TIPGe-Pn before (black trace); and after solvent-vapor annealing (SVA) and thermal annealing (TA), and of an aligned drop-cast thin film (blue, red, and orange traces, respectively). Polarized optical micrographs of (b) a spun-cast TIPGe-Pn film, (c) a spun-cast TIPGe-Pn film after SVA, (d) a spun-cast TIPGe-Pn film after TA, and (e) an aligned drop-cast TIPGe-Pn thin film.

as illustrated in the crystal structure shown in Figure 1e, in which the interactions between the conjugated core and the side group are enhanced at the expense of π – π interactions between neighboring molecules. That TIPGe-Pn accesses several packing motifs, far more diverse compared to that accessed in TIPS-Pn, suggests that the *electronic character*, rather than simply the size, of the side group significantly impacts their solid-state structural development. While the radii of the side groups of TIPS- and TIPGe-Pn are similar, the enhanced electron density on the TIPGe side group allows for access of the more stable herringbone and slip-stack packing motifs relative to the native brickwork packing in TIPS-Pn.

To further explore the structural phase space of TIPGe-Pn, spin-coating and aligned drop-casting⁴¹ were employed to produce thin films, and postdeposition thermal annealing (TA) and solvent-vapor annealing (SVA), previously shown to induce polymorphic transformations in a wide range of molecular semiconductors,^{19,21,42} were employed to assess whether we can access additional packing diversity in TIPGe-Pn. The ultraviolet–visible (UV–vis) absorption spectra of as-cast, TA and SVA spun-cast, and aligned drop-cast TIPGe-Pn thin films are shown in Figure 2a. The thickness of spun-cast and aligned drop-cast films were measured via ellipsometry and atomic force microscopy (AFM), respectively, and were found to be 64 ± 3 and 127 ± 15 nm. As the films and ribbons are tens or hundreds of nanometers thick, it is unlikely these are thin-film phases, as substrate-induced and thin-film phases in the literature typically appear in films that are on the order of several monolayers.⁴³ As-spun thin films of TIPGe-Pn are optically featureless, as shown in Figure 2b, and the corresponding UV–vis spectrum exhibits its peak absorbance at 649 nm, with secondary features resembling vibronic progression in solution at 598 and 553 nm. The absorption spectrum of the as-spun film closely resembles that of TIPGe-Pn in solution, with only a minor red shift, likely due to the change in dielectric constant of the surrounding medium. This

observation suggests that TIPGe-Pn in its as-spun film has limited-to-no electronic interactions among neighboring molecules in the solid state. Toluene-vapor annealing of spun-cast films produces small micrometer-sized crystalline grains, shown in Figure 2c. The vibronic features observed in the UV–vis spectrum of such a film are red-shifted relative to that in the spectrum of the as-spun film, with peak absorbances at 654, 600, and 555 nm. That this spectrum, too, closely resembles that of TIPGe-Pn in solution suggests that the SVA films also exhibit little electronic coupling. Thermal annealing at 150 °C induces TIPGe-Pn to crystallize, producing larger grains, as shown in Figure 2d, and further red shifts the vibronic features in its UV–vis spectrum by approximately 20 nm relative to those in the spectrum of the as-spun film, to peak absorbances of 671, 618, and 568 nm. We speculate this progressive red shift of peak absorbances in the spectra of the as-spun, spun-cast SVA, and spun-cast TA films is a result of increasing extents of intermolecular coupling in the solid state with postdeposition processing. Supporting this claim are DFT calculations that we had performed on the bulk slip-stack, herringbone, and brickwork packings. These calculations, shown in Figure S2, reveal a positive correlation between the average HOMO–HOMO and LUMO–LUMO electronic coupling, or intermolecular coupling, for dimer pairs of TIPGe-Pn and the extent of red-shift, going from the herringbone to the slip-stack to the brickwork structure. We thus infer that the red-shift observed in absorption spectra of TIPGe-Pn thin films, from as-spun to spun-cast SVA to spun-cast TA, to be due to increased intermolecular coupling in the solid-state. This inference, however, should be taken with some caution, as electronic coupling is computed between one-electron wave functions and the excited states accounting for all electrons in the system. Because the nature of optical excitation and the effect induced by static polarization varies from molecule to molecule (e.g., the degree of excited-state delocalization could differ depending on the packing arrange-

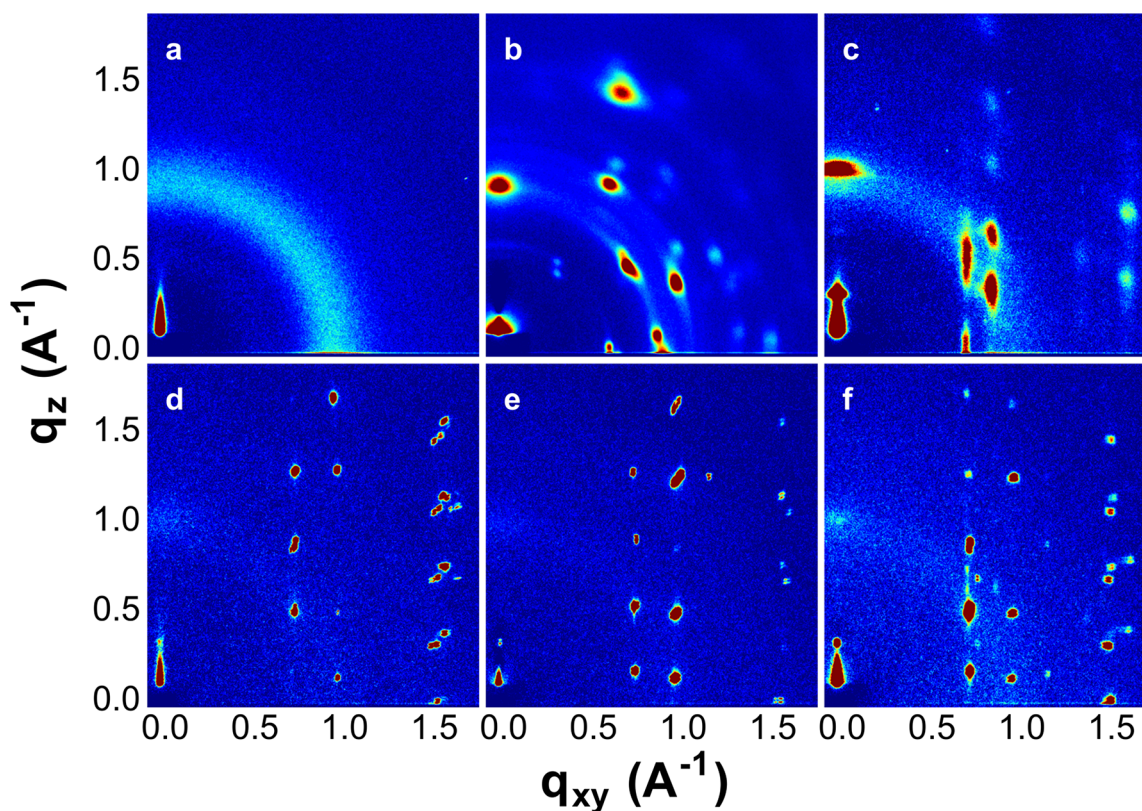


Figure 3. Grazing-incidence X-ray diffraction pattern of (a) a spun-cast thin film of TIPGe-Pn. X-ray patterns of spun-cast films after (b) TA and (c) SVA. X-ray patterns of aligned drop-cast TIPGe-Pn before (d) and after TA (e) and SVA (f).

ment), our conclusion here is also likely specific to TIPGe-Pn and not generalizable to other molecular systems.

Aligned drop-casting produced millimeters-long ribbons, as shown in Figure 2e. Energy dispersive X-ray (EDX) spectroscopy was performed on aligned drop-cast films, specifically scanning for germanium in the low-lying regions. The results, which are shown in Figure S3 and summarized in Table S2, confirm that TIPGe-Pn ribbons are isolated. The UV-vis spectrum for one such aligned drop-cast film, Figure 2a, is marked with red-shifted vibronic features, relative to spun-cast films, whose relative absorbances are inverted, such that the most absorptive feature is at the lowest wavelength compared to the other features in the spectrum. We do not observe any changes in the absorption spectra of aligned drop-cast films upon TA or SVA, suggesting that aligned drop-cast films do not further undergo structural evolution with postdeposition processing. Following the correlation between red shift and absorbance in bulk packing motifs, and inferred for spun-cast films, we expect aligned drop-cast films of TIPGe-Pn to exhibit higher yet intermolecular coupling compared to spun-cast films. Further, we note that an inversion in the relative absorbances of the vibronic features is observed in aligned drop-cast thin films. This observation is consistent with an increase in electronic coupling and delocalization of the electronic states. Calculations by Sharifzadeh et al.⁴⁴ on TIPS-Pn showed that both delocalization and the presence of multiple transitions can cause crystals having a brickwork packing motif to display polarization-dependent absorption, in which the relative absorbances of the transitions differ from that of a single molecule. Further, moderate changes to the intermolecular distance of pentacene can drastically change the extent of delocalization, highlighting the importance of packing

on electron delocalization in the solid-state. This analysis in TIPS-Pn highlights the importance of spacing and packing of adjacent TIPS-Pn molecules in the solid state on electron delocalization, which can impart changes to the optical properties of the material. We therefore believe the changes present in the optical spectra to be the result of differences in the intermolecular packing of TIPGe-Pn as a function of processing conditions.

To characterize the solid-state structures accessed in thin films, grazing-incidence X-ray diffraction (GIXD) was performed at the Cornell High Energy Synchrotron Source (CHESS), and the resulting 2D GIXD patterns are shown in Figure 3. Figure 3a shows a diffuse halo, indicating that the spun-cast film is amorphous with no long-range order. The observation of amorphous films is consistent with results from our UV-vis measurements; as-spun thin films of TIPGe-Pn exhibit features to suggest that the molecules are electronically isolated from each other. Postdeposition TA and SVA induces crystallization; we observe sharp reflections in the GIXD images of these films in Figure 3b,c that indicate the presence of preferentially oriented crystalline domains. While we are still in the process of identifying the crystal structures that these films adopt (identification of crystal structures from thin-film GIXD is difficult given the limited number of reflections), the reflections in the GIXD patterns in Figures 3b,c do not match those of the three known bulk crystal structures that are shown in Figure 1. It thus appears that postdeposition annealing of spun-cast films of TIPGe-Pn accesses yet distinct crystal structures. Spun-cast TA films exhibit an out-of-plane *d*-spacing of approximately 16.5 Å, which is similar to the out-of-plane characteristic spacing observed in aligned drop-cast films and the side-group to side-group distance of TIPGe-Pn.

Therefore, TIPGe-Pn likely adopts an edge-on orientation in spun-cast TA films. Spun-cast SVA TIPGe-Pn films exhibit an out-of-plane d -spacing of approximately 6.2 Å. We postulate that the tighter d -spacing observed is a result of a different out-of-plane orientation compared to the spun-cast TA and aligned drop-cast films.

Figure 3d–f shows the GIXD patterns for as-cast, TA, and SVA aligned drop-cast films, which are composed of highly oriented and aligned single-crystalline ribbons (Figure 2e). These films all access the brickwork packing motif, with unit-cell lattice parameters that vary only slightly with post-deposition processing, as summarized in Table S3. Unit-cell lattice parameters for aligned drop-cast films were obtained using the Diffraction Pattern Calculator (DPC) toolkit.⁴⁵ The crystal structures accessed in the aligned drop-cast films adopt an edge-on orientation and are nearly identical to the bulk crystal structure of TIPGe-Pn that adopts the brickwork packing motif; this similarity is also observed in the calculated slip parameters for the drop-cast film and the bulk crystal of TIPGe-Pn, as summarized in Table S4. Aligned drop-casting of TIPGe-Pn induces directional solvent evaporation, which imposes macroscopic preferential orientation in the crystalline domains, with the crystalline ribbons growing in the direction of the solvent evaporation front. To determine the orientation of crystalline ribbons grown by aligned drop-casting, as shown in Figure 2e, we collected GIXD patterns with incident X-rays normal and parallel to the long axis of the crystals, the patterns of which are shown in Figure S4a,b. Indexing the reflections from these GIXD patterns against the crystal structure sheds light on the preferential orientation. Upon aligned drop-casting, TIPGe-Pn is preferentially oriented with its (001) plane out-of-plane, as evidenced by the reflection at $q_z = 0.39 \text{ \AA}^{-1}$, $q_{xy} = 0 \text{ \AA}^{-1}$ in Figure 3d. By rotating the sample 90° in-plane, both the (0 1 l) and (1 0 l) families of reflections are captured in GIXD scans perpendicular and parallel to the ribbon long-axis, respectively, shown in Figure S4c,d. As such, we determined that the a -axis of the unit cell, or the direction along which π -stacking takes place, is coincident with the long-axis of the ribbons, as is typical for many organic semiconductors.^{42,46,47} Encouraged by their single-crystalline nature and two-dimensional brickwork-type packing motif, we assessed the charge transport characteristics by fabricating TIPGe-Pn thin-film transistors with ribbons spanning the active channels.

Organic field-effect transistors (OFETs) were produced using spun and aligned drop-cast thin films as active layers in a bottom-gate, bottom-contact configuration. Oriented drop-cast films were grown over PFBT-treated bottom contacts such that the ribbons grew across the device channel, as shown in Figure 4a. This configuration allowed us to probe transport along the a -axis of the crystal structure, as shown in Figure 4b. Representative transfer characteristics of transistors with aligned drop-cast active layers collected in the saturation regime ($V_{DS} = -80 \text{ V}$) are shown in Figure 4b, and representative output curves are shown in Figure S5a.

Devices comprising aligned drop-cast ribbons exhibit hole mobilities of $0.72 \pm 0.21 \text{ cm}^2 \text{ V}^{-1} \text{ s}^{-1}$, with a maximum mobility of $1.33 \text{ cm}^2 \text{ V}^{-1} \text{ s}^{-1}$, exceeding the benchmark performance of amorphous silicon transistors. Device characteristics are summarized in Table 2. As the ribbons produced via aligned drop-casting do not completely cover the transistor channel, the width of the crystals in each device channel was measured via optical microscopy and used to calculate the

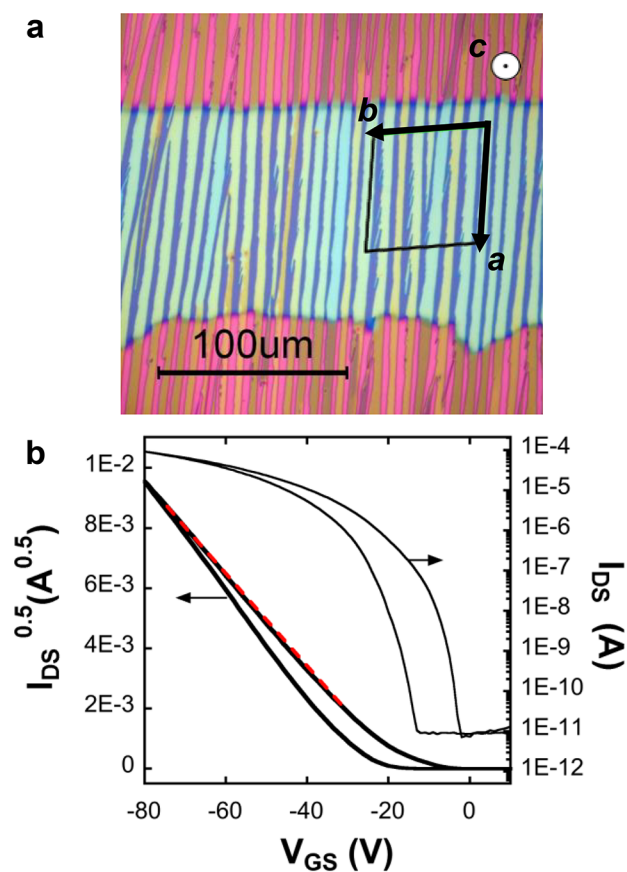


Figure 4. (a) Optical micrograph of a transistor channel, highlighting alignment of TIPGe-Pn ribbons obtained upon aligned drop-casting. Unit-cell orientation is illustrated with respect to ribbon orientation. The c -axis is oriented out-of-plane, with the a -axis oriented along the long axis of the ribbons, which is also the direction of the solvent evaporation front. (b) Transfer characteristics of thin-film transistors with such TIPGe-Pn ribbons at $V_{DS} = -80 \text{ V}$. The portion of the transfer curve that was fit for TIPGe-Pn drop-cast devices is highlighted with the red dashed line, from -30 to -75 V .

Table 2. Summary of Device Characteristics for TIPS- and TIPGe-Pn Transistors

compound	deposition	post-deposition processing	μ ($\text{cm}^2/\text{V/s}$)	V_T (V)
TIPGe-Pn	spun-cast ^a	+ SVA	no field effect	no field effect
	spun-cast ^a	+ TA	$(1.1 \pm 0.2) \times 10^{-5}$	-28.6 ± 0.6
	drop-cast ^b	as-cast	0.72 ± 0.21	-26 ± 7
TIPS ⁴⁸	drop-cast	as-cast	0.65 ± 0.35	3 ± 5

^aCharacteristics are averaged across 20 devices over 3 different substrates. ^bCharacteristics are averaged across 20 devices over 2 different substrates.

mobility. The threshold voltage for these devices was found to be $-26 \pm 7 \text{ V}$. Measurements were obtained and averaged across 20 devices. Despite increasing the concentration of the solution or employing different solvents, complete coverage could not be obtained, and therefore charge transport along the b -axis could not be measured.

The mobility for devices with aligned drop-cast TIPGe-Pn ribbons along the a -axis is very similar to that of TIPS-Pn transistors with thin-film active layers produced via aligned

drop-casting ($0.65 \pm 0.35 \text{ cm}^2 \text{ V}^{-1} \text{ s}^{-1}$).⁴⁸ The similarity in mobilities accessed for devices with TIPS- and TIPGe-Pn active layers suggests that the brickwork packing motif of the pentacene conjugated core accessed in both plays a significant role in determining the field-effect mobility. Differences in the side group, while facilitating the access of new polymorphs in the case of TIPGe-Pn, have little impact on the overall performance of the device for active layers of the same packing motif. The short, long, and vertical axis slips for the TIPS- and TIPGe-Pn brickwork packing motifs, included in Table 2, are very similar, indicating similar backbone orientation and electronic coupling in these structures and highlighting the importance of the packing motif and π -orbital overlap.

In comparison to aligned drop-cast TIPGe-Pn devices, transistors with spun-cast and annealed active layers exhibited poor or no measurable field-effect characteristics. SVA of active layers did not improve device performance, whereas TA of active layers produced hole mobilities of $(1.1 \pm 0.2) \times 10^{-5} \text{ cm}^2 \text{ V}^{-1} \text{ s}^{-1}$ with threshold voltages of $-29 \pm 7 \text{ V}$. Representative output and transfer curves for spun-cast, TA OTFTs are included in Figures S5b and S6, respectively. The stark difference in mobilities for devices with spun-cast TIPGe-Pn films relative to those with aligned drop-cast active layers can primarily be attributed to the different crystal structures accessed in each case, and secondarily to the presence of grain boundaries, which exist in both spun-cast, annealed films but not in the single-crystalline drop-cast ribbons. While the crystal structures of spun-cast, annealed TIPGe-Pn polymorphs are as yet unsolved, we suspect these structures to have poor π -orbital overlap in plane. We hypothesize these new polymorphs may adopt a one-dimensional slip-stack or a herringbone packing motif, both of which have limited face-to-face, or π -stacking, interactions. This assertion is consistent with observations previously made with TES-Pn, which adopts a one-dimensional slip-stack packing motif. Transistors with TES-Pn ribbons exhibit mobilities that are an order of magnitude lower than transistors comprising TIPS-Pn ribbons.⁴⁹ In the absence of grain boundaries, this discrepancy in mobility and charge transport anisotropy must stem from the one-dimensional, as opposed to two-dimensional, packing motif in TES-Pn compared to TIPS-Pn.⁴⁹ The comparatively low mobilities in spun-cast TIPGe-Pn devices, despite a crystalline active layer, suggest that TIPGe-Pn processed under these conditions likely adopts a slip-stack packing motif not dissimilar to that in TES-Pn or 6,13-bis(trimethylsilylethynyl)pentacene (TMS-Pn).

CONCLUSIONS

The solid-state packing of functionalized acenes in the bulk and in thin films is not only dependent on the size of the side group but also upon the electron density of the side group, as demonstrated in this comparative study between TIPGe-Pn and TIPS-Pn. While the radius of the side group increases by less than 2%, the electron density increases by 21% with substitution of germanium for silicon. This increased electron density resulted in a significantly wider phase space for TIPGe-Pn, allowing access to several distinct polymorphs in single crystals and thin films that are not accessible in TIPS-Pn. Access to the new polymorphs in thin films is controlled by processing conditions in TIPGe-Pn. We access a brickwork packing motif through aligned drop-casting, or two as-yet undetermined polymorphs through TA or SVA of spun-cast films. Devices with aligned drop-cast TIPGe-Pn thin-film active layers produce average mobilities of $0.72 \pm 0.21 \text{ cm}^2 \text{ V}^{-1} \text{ s}^{-1}$,

with maximum mobilities of $1.33 \text{ cm}^2 \text{ V}^{-1} \text{ s}^{-1}$. The ability to access a rich and diverse structural landscape by employing more subtle substitutions that do not disrupt the electronic properties of the core, as evidenced by the similarities in charge transport properties of brickwork TIPS- and TIPGe-Pn, may provide additional opportunities for structural optimization in future organic electronic materials. Further development of the relative importance of alkyl side-chain size and electron density on the accessible packing motifs of organic semiconductors will provide improved design rules to guide the synthesis of promising next-generation molecules for electronic devices.

ASSOCIATED CONTENT

Supporting Information

The Supporting Information is available free of charge on the ACS Publications website at DOI: [10.1021/acs.chemmater.9b00546](https://doi.org/10.1021/acs.chemmater.9b00546).

Synthesis and crystal growth; device fabrication and testing; details of DFT calculations; DSC thermograms; supplemental GIXD patterns; device testing curves; crystal structures and details (PDF)

AUTHOR INFORMATION

Corresponding Author

*E-mail: lloo@princeton.edu.

ORCID

John E. Anthony: [0000-0002-8972-1888](https://orcid.org/0000-0002-8972-1888)

Chad Risko: [0000-0001-9838-5233](https://orcid.org/0000-0001-9838-5233)

Yueh-Lin Loo: [0000-0002-4284-0847](https://orcid.org/0000-0002-4284-0847)

Funding

J.C.S. and Y.-L.L. acknowledge National Science Foundation (NSF) funding under Award DMR-1627453, as well as that from the Princeton Center for Complex Materials, a MRSEC supported by the NSF under Award DMR-1420541. A portion of this work was conducted at the Cornell High Energy Synchrotron Source (CHESS), which is supported by the NSF under Award DMR-1332208. J.E.A. and C.R. acknowledge the NSF under Award DMR-1627428. Supercomputing resources on the Lipscomb High Performance Computing Cluster were provided by the University of Kentucky Information Technology Department and Center for Computational Sciences (CCS).

Notes

The authors declare no competing financial interest.

ACKNOWLEDGMENTS

S.P. acknowledges the NSF MRI Program under award CHE-1625732.

ABBREVIATIONS

DFT, density functional theory; GIXD, grazing incidence X-ray diffraction; UV-vis, UV-visible; DSC, differential scanning calorimetry; SVA, solvent-vapor annealing; TA, thermal annealing; CCDC, Cambridge Crystallographic Data Centre; CHESS, Cornell High Energy Synchrotron Source

REFERENCES

- (1) Threlfall, T. L. Analysis of Organic Polymorphs. *Analyst* **1995**, *120*, 2435–2460.

- (2) Kuhnert-Brandstfitter, M.; Riedmann, M. Thermal Analytical and Infrared Spectroscopic Investigations on Polymorphic Organic Compounds-I. *Microchim. Acta* **1987**, *92*, 107–120.
- (3) Hunter, C. A.; Sanders, J. K. M. The Nature of Pi-Pi Interactions. *J. Am. Chem. Soc.* **1990**, *112*, 5525–5534.
- (4) Guthrie, S. M.; Smilgies, D. M.; Giri, G. Controlling Polymorphism in Pharmaceutical Compounds Using Solution Shearing. *Cryst. Growth Des.* **2018**, *18*, 602–606.
- (5) Mannsfeld, S. C. B.; Virkar, A.; Reese, C.; Toney, M. F.; Bao, Z. Precise Structure of Pentacene Monolayers on Amorphous Silicon Oxide and Relation to Charge Transport. *Adv. Mater.* **2009**, *21*, 2294–2298.
- (6) Wang, X.; Garcia, T.; Monaco, S.; Schatschneider, B.; Marom, N. Effect of Crystal Packing on the Excitonic Properties of Rubrene Polymorphs. *CrystEngComm* **2016**, *18*, 7353–7362.
- (7) Yu, L.; Li, X.; Pavlica, E.; Koch, F. P. V.; Portale, G.; Da Silva, I.; Loth, M. A.; Anthony, J. E.; Smith, P.; Bratina, G.; et al. Influence of Solid-State Microstructure on the Electronic Performance of 5,11-Bis(Triethylsilyl)ethynyl Anthradithiophene. *Chem. Mater.* **2013**, *25*, 1823–1828.
- (8) Mei, J.; Diao, Y.; Appleton, A. L.; Fang, L.; Bao, Z. Integrated Materials Design of Organic Semiconductors for Field-Effect Transistors. *J. Am. Chem. Soc.* **2013**, *135*, 6724–6746.
- (9) Teixeira da Rocha, C.; Haase, K.; Zheng, Y.; Löffler, M.; Hamsch, M.; Mannsfeld, S. C. B. Solution Coating of Small Molecule/Polymer Blends Enabling Ultralow Voltage and High-Mobility Organic Transistors. *Adv. Electron. Mater.* **2018**, *4*, 1800141.
- (10) DeLongchamp, D. M.; Vogel, B. M.; Jung, Y.; Gurau, M. C.; Richter, C. A.; Kirillov, O. A.; Obrzut, J.; Fischer, D. A.; Sambasivan, S.; Richter, L. J.; et al. Variations in Semiconducting Polymer Microstructure and Hole Mobility with Spin-Coating Speed. *Chem. Mater.* **2005**, *17*, 5610–5612.
- (11) Chen, J.; Shao, M.; Xiao, K.; Rondinone, A. J.; Loo, Y.-L.; Kent, P. R. C.; Sumpter, B. G.; Li, D.; Keum, J. K.; Diemer, P. J.; et al. Solvent-Type-Dependent Polymorphism and Charge Transport in a Long Fused-Ring Organic Semiconductor. *Nanoscale* **2014**, *6*, 449–456.
- (12) Diao, Y.; Tee, B. C. K.; Giri, G.; Xu, J.; Kim, D. H.; Becerril, H. A.; Stoltenberg, R. M.; Lee, T. H.; Xue, G.; Mannsfeld, S. C. B.; et al. Solution Coating of Large-Area Organic Semiconductor Thin Films with Aligned Single-Crystalline Domains. *Nat. Mater.* **2013**, *12*, 665–671.
- (13) Yuan, Y.; Giri, G.; Ayzner, A. L.; Zoombelt, A. P.; Mannsfeld, S. C. B.; Chen, J.; Nordlund, D.; Toney, M. F.; Huang, J.; Bao, Z. Ultra-High Mobility Transparent Organic Thin Film Transistors Grown by an off-Centre Spin-Coating Method. *Nat. Commun.* **2014**, *5*, 3005.
- (14) Diao, Y.; Lenn, K. M.; Lee, W.-Y.; Blood-Forsythe, M. A.; Xu, J.; Mao, Y.; Kim, Y.; Reinspach, J. A.; Park, S.; Aspuru-Guzik, A.; et al. Understanding Polymorphism in Organic Semiconductor Thin Films through Nanoconfinement. *J. Am. Chem. Soc.* **2014**, *136*, 17046–17057.
- (15) Giri, G.; Park, S.; Vosgueritchian, M.; Shulaker, M. M.; Bao, Z. High-Mobility, Aligned Crystalline Domains of TIPS-Pentacene with Metastable Polymorphs Through Lateral Confinement of Crystal Growth. *Adv. Mater.* **2014**, *26*, 487–493.
- (16) Giri, G.; Li, R.; Smilgies, D. M.; Li, E. Q.; Diao, Y.; Lenn, K. M.; Chiu, M.; Lin, D. W.; Allen, R.; Reinspach, J. A.; et al. One-Dimensional Self-Confinement Promotes Polymorph Selection in Large-Area Organic Semiconductor Thin Films. *Nat. Commun.* **2014**, *5*, 3573.
- (17) Sele, C. W.; Kjellander, B. K. C.; Niesen, B.; Thornton, M. J.; van der Putten, J. B. P. H.; Myny, K.; Wöndergem, H. J.; Moser, A.; Resel, R.; van Breemen, A. J. J. M.; et al. Controlled Deposition of Highly Ordered Soluble Acene Thin Films: Effect of Morphology and Crystal Orientation on Transistor Performance. *Adv. Mater.* **2009**, *21*, 4926–4931.
- (18) Chen, J.; Anthony, J. E.; Martin, D. C. Thermally Induced Solid-State Phase Transition of Bis(Triisopropylsilyl)ethynyl Pentacene Crystals. *J. Phys. Chem. B* **2006**, *110*, 16397–16403.
- (19) Hiszpanski, A. M.; Lee, S. S.; Wang, H.; Woll, A. R.; Nuckolls, C.; Loo, Y.-L. Post-Deposition Processing Methods To Induce Preferential Orientation in Contorted Hexabenzocoronene Thin Films. *ACS Nano* **2013**, *7*, 294–300.
- (20) Hiszpanski, A. M.; Baur, R. M.; Kim, B.; Tremblay, N. J.; Nuckolls, C.; Woll, A. R.; Loo, Y.-L. Tuning Polymorphism and Orientation in Organic Semiconductor Thin Films via Post-Deposition Processing. *J. Am. Chem. Soc.* **2014**, *136*, 15749–15756.
- (21) Purdum, G. E.; Yao, N.; Woll, A. R.; Gessner, T.; Weitz, R. T.; Loo, Y.-L. Understanding Polymorph Transformations in Core-Chlorinated Naphthalene Diimides and Their Impact on Thin-Film Transistor Performance. *Adv. Funct. Mater.* **2016**, *26*, 2357–2364.
- (22) Hiszpanski, A. M.; Dsilva, C. J.; Kevrekidis, I. G.; Loo, Y.-L. Data Mining for Parameters Affecting Polymorph Selection in Contorted Hexabenzocoronene Derivatives. *Chem. Mater.* **2018**, *30*, 3330–3337.
- (23) Purdum, G. E.; Telesz, N. G.; Jarolimek, K.; Ryno, S. M.; Gessner, T.; Davy, N. C.; Petty, A. J.; Zhen, Y.; Shu, Y.; Facchetti, A.; et al. Presence of Short Intermolecular Contacts Screens for Kinetic Stability in Packing Polymorphs. *J. Am. Chem. Soc.* **2018**, *140*, 7519–7525.
- (24) Anthony, J. E.; Brooks, J. S.; Eaton, D. L.; Parkin, S. R. Functionalized Pentacene: Improved Electronic Properties from Control of Solid-State Order. *J. Am. Chem. Soc.* **2001**, *123*, 9482–9483.
- (25) Hiszpanski, A. M.; Woll, A. R.; Kim, B.; Nuckolls, C.; Loo, Y.-L. Altering the Polymorphic Accessibility of Polycyclic Aromatic Hydrocarbons with Fluorination. *Chem. Mater.* **2017**, *29*, 4311–4316.
- (26) Hailey, A. K.; Petty, A. J.; Washbourne, J.; Thorley, K. J.; Parkin, S. R.; Anthony, J. E.; Loo, Y.-L. Understanding the Crystal Packing and Organic Thin-Film Transistor Performance in Isomeric Guest–Host Systems. *Adv. Mater.* **2017**, *29*, 1700048.
- (27) Hallani, R. K.; Thorley, K. J.; Mei, Y.; Parkin, S. R.; Jurchescu, O. D.; Anthony, J. E. Structural and Electronic Properties of Crystalline, Isomerically Pure Anthradithiophene Derivatives. *Adv. Funct. Mater.* **2016**, *26*, 2341–2348.
- (28) Lei, T.; Wang, J. Y.; Pei, J. Roles of Flexible Chains in Organic Semiconducting Materials. *Chem. Mater.* **2014**, *26*, 594–603.
- (29) Ha, J. S.; Kim, K. H.; Choi, D. H. 2,5-Bis(2-Octyldodecyl)pyrrolo[3,4-c]pyrrole-1,4-(2H,5H)-Dione-Based Donor-Acceptor Alternating Copolymer Bearing 5,5'-Di(Thiophen-2-yl)-2,2'-Biselenophene Exhibiting 1.5 Cm²V⁻¹s⁻¹ Hole Mobility in Thin-Film Transistors. *J. Am. Chem. Soc.* **2011**, *133*, 10364–10367.
- (30) Himmelberger, S.; Duong, D. T.; Northrup, J. E.; Rivnay, J.; Koch, F. P. V.; Beckingham, B. S.; Stingelin, N.; Segalman, R. A.; Mannsfeld, S. C. B.; Salleo, A. Role of Side-Chain Branching on Thin-Film Structure and Electronic Properties of Polythiophenes. *Adv. Funct. Mater.* **2015**, *25*, 2616–2624.
- (31) He, T.; Stolte, M.; Würthner, F. Air-Stable n-Channel Organic Single Crystal Field-Effect Transistors Based on Microribbons of Core-Chlorinated Naphthalene Diimide. *Adv. Mater.* **2013**, *25*, 6951–6955.
- (32) He, T.; Stolte, M.; Burschka, C.; Hansen, N. H.; Musiol, T.; Kälblein, D.; Pflaum, J.; Tao, X.; Brill, J.; Würthner, F. Single-Crystal Field-Effect Transistors of New Cl 2-NDI Polymorph Processed by Sublimation in Air. *Nat. Commun.* **2015**, *6*, 5954.
- (33) Schulz, G. L.; Fischer, F. S. U.; Trefz, D.; Melnyk, A.; Hamidi-Sakr, A.; Brinkmann, M.; Andrienko, D.; Ludwigs, S. The PCPDTBT Family: Correlations between Chemical Structure, Polymorphism, and Device Performance. *Macromolecules* **2017**, *50*, 1402–1414.
- (34) Anthony, J. E.; Eaton, D. L.; Parkin, S. R. A Road Map to Stable, Soluble, Easily Crystallized Pentacene Derivatives. *Org. Lett.* **2002**, *4*, 15–18.
- (35) Thorley, K. J.; Finn, T. W.; Jarolimek, K.; Anthony, J. E.; Risko, C. Theory-Driven Insight into the Crystal Packing of Trialkylsilyl-ethynyl Pentacenes. *Chem. Mater.* **2017**, *29*, 2502–2512.
- (36) Ciavatti, A.; Basiricò, L.; Fratelli, I.; Lai, S.; Cosseddu, P.; Bonfiglio, A.; Anthony, J. E.; Fraboni, B. Boosting Direct X-Ray

Detection in Organic Thin Films by Small Molecules Tailoring. *Adv. Funct. Mater.* **2018**, 1806119.

(37) Zhang, H.; Yao, Y.; Payne, M. M.; Anthony, J. E.; Brill, J. W. Thermal Diffusivities of Functionalized Pentacene Semiconductors. *Appl. Phys. Lett.* **2014**, 105, 073302.

(38) Allen, C. F. H.; Bell, A. Action of Grignard Reagents on Certain Pentacenequinones, 6,13-Diphenylpentacene. *J. Am. Chem. Soc.* **1942**, 64, 1253–1260.

(39) Funk, R. L.; Young, E. R. R.; Williams, R. M.; Flanagan, M. F.; Cecil, T. L. Photochemical Cycloaromatization Reactions of Ortho-Dialkynylarenes: A New Class of DNA Photocleaving Agents. *J. Am. Chem. Soc.* **1996**, 118, 3291–3292.

(40) Miller, G. P.; Mack, J.; Briggs, J. π -Stacking Interactions in Cis-Bisfullerene[60] Adducts of 6,13-Disubstituted Pentacenes. *Org. Lett.* **2000**, 2, 3983–3986.

(41) Nakayama, K.; Hirose, Y.; Soeda, J.; Yoshizumi, M.; Uemura, T.; Uno, M.; Li, W.; Kang, M. J.; Yamagishi, M.; Okada, Y.; et al. Patternable Solution-Crystallized Organic Transistors with High Charge Carrier Mobility. *Adv. Mater.* **2011**, 23, 1626–1629.

(42) Lee, S. S.; Tang, S. B.; Smilgies, D. M.; Woll, A. R.; Loth, M. A.; Mativetsky, J. M.; Anthony, J. E.; Loo, Y.-L. Guiding Crystallization around Bends and Sharp Corners. *Adv. Mater.* **2012**, 24, 2692–2698.

(43) Jones, A. O. F.; Chattopadhyay, B.; Geerts, Y. H.; Resel, R. Substrate-Induced and Thin-Film Phases: Polymorphism of Organic Materials on Surfaces. *Adv. Funct. Mater.* **2016**, 26, 2233–2255.

(44) Sharifzadeh, S.; Wong, C. Y.; Wu, H.; Cotts, B. L.; Kronik, L.; Ginsberg, N. S.; Neaton, J. B. Relating the Physical Structure and Optoelectronic Function of Crystalline TIPS-Pentacene. *Adv. Funct. Mater.* **2015**, 25, 2038–2046.

(45) Hailey, A. K.; Hiszpanski, A. M.; Smilgies, D.-M.; Loo, Y.-L. The Diffraction Pattern Calculator (DPC) Toolkit: A User-Friendly Approach to Unit-Cell Lattice Parameter Identification of Two-Dimensional Grazing-Incidence Wide-Angle X-Ray Scattering Data. *J. Appl. Crystallogr.* **2014**, 47, 2090–2099.

(46) Schmidt-Mende, L.; Fechtenkötter, A.; Müllen, K.; Moons, E.; Friend, R. H.; MacKenzie, J. D. Self-Organized Discotic Liquid Crystals for High-Efficiency Organic Photovoltaics. *Science (Washington, DC, U. S.)* **2001**, 293, 1119–1122.

(47) Percec, V.; Glodde, M.; Bera, T. K.; Miura, Y.; Shiyonovskaya, I.; Singer, K. D.; Balagurusamy, V. S. K.; Heiney, P. A.; Schnell, I.; Rapp, A.; et al. Self-Organization of Supramolecular Helical Dendrimers into Complex Electronic Materials. *Nature* **2002**, 419, 384–387.

(48) Park, S. K.; Jackson, T. N.; Anthony, J. E.; Mourey, D. A. High Mobility Solution Processed 6,13-Bis(Triisopropyl-Silylethynyl) Pentacene Organic Thin Film Transistors. *Appl. Phys. Lett.* **2007**, 91, 063514.

(49) James, D. T.; Frost, J. M.; Wade, J.; Nelson, J.; Kim, J. S. Controlling Microstructure of Pentacene Derivatives by Solution Processing: Impact of Structural Anisotropy on Optoelectronic Properties. *ACS Nano* **2013**, 7, 7983–7991.